Proceeding of the IEEE
International Conference on Robotics and Biomimetics
Dali, China, December 2019

Biomimetic Stretchable Sensor Resembling Shar-Pei Crumples with 2D Materials towards Collaborative Robotic Minimally Invasive Procedures

Parita Sanghani [1], Catherine Jiayi Cai [1] and Ting-Hsiang Chang[2], Benjamin Delecourt[3], Chwee Ming Lim[4], Po-Yen Chen[2,*], Hongliang Ren[1,*]

[1] Department of Biomedical Engineering, National University of Singapore, 117576, Singapore
[2] Department of Chemical and Biomolecular Engineering, National University of Singapore, 119077, Singapore
[3] Department of Biomedical Engineering, Institute Polytechnique de Grenoble, France
[4] Department of Otolaryngology, Singapore General Hospital
*Correspondence: checp@nus.edu.sg and hlren@ieee.org

***Abstract* - For the purpose of collision avoidance, medical robots can utilize tactile sensors with 2D materials including reduced graphene oxide rGO and MXene electrodes that are stretchable like the skin of humans. When the electrode surface is visualized using scanning electrode microscope (SEM), the surface morphologies have wrinkles like those found on Shar Pei dog faces. This study aims to examine the biomimetic similarity between the 2D crumples in SEM images of the electrode surface and in the images of Shar-Pei dog faces. The similarity in 2D crumples was assessed by computing the angles made by the crumples and analyzing its distribution. This study demonstrates that there is a biomimetic similarity between the dog face and the SEM images of the rGO and MXene electrodes. This implies similar stretchable functionalities and protective principles out of the crumple geometry of the sensors and Shar-Pei skins.**

Index Terms - wrinkle and crumple structures; MXene electrode; reduced graphene oxide electrode; biomimetic similarity; surgical robotics.

I. INTRODUCTION

Engineers have conventionally made use of rigid materials for fabricating surgical robots. However, flexible robots are of prime importance as they can mimic natural flexible systems and perform more diversified tasks in confined curvilinear spaces. The recent developments in the field of biorobotics and advanced materials have led to the creation of flexible and soft robots.

To further improve machine-environment interaction, research had been carried out to equip these soft robots with tactile and pressure sensing capabilities. These can help surgeons evaluate anatomical structures and determine the appropriate amount of force applied for safe tissue manipulation [1,2]. It has been shown that the presence of such sensing capabilities during robotic-assisted surgery can improve surgical performance, reduce completion time, improves the economy of force exertion and hence lesser trauma to the manipulated tissue [3-5]. In addition, having tactile feedback can further aid surgeons in detecting possible collisions between instruments or between tissue and instruments that can cause unnecessary damage and trauma [6].

In order to be compatible with the application of soft robotics, it is desirable for the pressure sensor to be compliant such that it is able to withstand repeated and reversible bending and stretching with minimal loss of sensitivity and electrical properties [7]. Hence, flexible and stretchable sensing elements are highly desirable. Recently, anatomically thin conducting 2D materials have emerged as alternative materials for the use of flexible electronics due to their high electrical conductivity, low density, large surface area, high mechanical strength and environmental friendliness [8-10].

While 2D materials are intrinsically flexible, they are not intrinsically elastic. Hence, there is a need to confer stretchability by appropriate geometrical arrangement and structural design of the materials. One common approach is to perform buckling, in which a conducting film is first deposited on a pre-strained substrate [11]. When the substrate undergoes relaxation, the pre-strain is released and the formation of sinusoidal wavy patterns is induced onto the conducting film. These wavy patterns appear similar to wrinkles or buckles. It has also been found that the buckling technique can create complex surface topographies and 3D architectures of 2D materials [9], which can improve the sensitivity and response speed of pressure sensors as compared to planar structures [12,13]. Several works have explored the use of wrinkled patterns in sensors [12-14]. These wrinkle-like patterns are greatly diverse in terms of morphology and are abundantly observed and inspired by nature, such as the cells, the brain and fingers [15]. However, to our knowledge, no work has been done to explore how specific biomimetic patterns can affect sensing patterns like stretchability, sensitivity and other parameters.

In our previous work, we had developed a stretchable pressure sensor by integrating the wrinkle architecture of active 2D materials onto a soft elastomeric substrate to achieve a bilayer structure with high mechanical stability and stretchability [16]. Stretchable reduced Graphene Oxide (rGO) and MXene electrodes were created and conferred with wrinkles and were found to exhibit high stretchability (~100%). Interestingly, we have also found it to exhibit strain insensitivity. Upon observation of the wrinkled patterns of the

978-1-7281-6321-5/19//$31.00 ©2019 IEEE

electrodes, we have found it to resemble that of a Shar-Pei dog skin. In domesticated animals, the Shar-Pei dog is a breed that is prized for its distinctive wrinkly skin [17]. These wrinkles act as a protection mechanism in the course of a fight, by allowing the skin to stretch and preventing injury to the organs. In this study, we are interested in investigating whether the interesting property of strain insensitivity is due to this specific biomimetic pattern. This being our preliminary study, we first aim to establish the biomimetic similarity between the wrinkled electrode surface and that of the Shar Pei dog skin.

The surface morphologies of the rGO and MXene films on the electrode were examined using a scanning electrode microscope (SEM). To examine the biomimetic similarity between the images obtained from the SEM images and Shar-Pei dog skin, there is a need for a method to quantify the behavioral biomimetic similarity. Our work introduces one way of describing those similarities by evaluating the 2D crumples obtained in the skin and the SEM images. The dog and SEM images are found to be composed of similar looking ripples. This similarity is analyzed by computing the angles of the ripples and curves in these images.

II. MATERIALS AND METHODS

To fabricate the electrodes, the methodology employed by Chen et al [12,18] to create stretchable 2D material-elastomer composites was executed. The manufacturing methodology involves wrinkling and crumpling of 2D material films (such as graphene or MXene) using mismatched mechanical deformation. This creates accordion-like composite structures that can be unfolded by in-plane mechanical deformations. This can effectively diminish the effective strain experienced by the 2D material when undergoing tension and bending and can hence undergo deformations without breaking or fracturing. The wrinkled films are then transferred onto flexible and elastic polymer substrates. In the earlier work, Chen et al [12] found that these 2D material-elastomer composites have demonstrated stable electrical conductivity, and are able to tolerate reversible deformations for up to 500 cycles without experiencing failure.

A. SEM Data

A scanning electron microscope (SEM) was utilized to obtain images of the surface morphology of the film on the sensor electrodes (16 SEM images of rGO sensors and 7 for MXene sensors in this study). On the other hand, 16 high-resolution Shar Pei dog images were collected to compare the wrinkles with those in the SEM images. Figure 1 shows some example images used in the study. The first row shows some examples of Shar Pei dog face images used in the study. The second row shows remarkable examples of SEM images of the surface of the rGO film on the electrode used in the study. The last row shows remarkable examples of SEM images of the surface of the MXene film on the electrode used in the study.

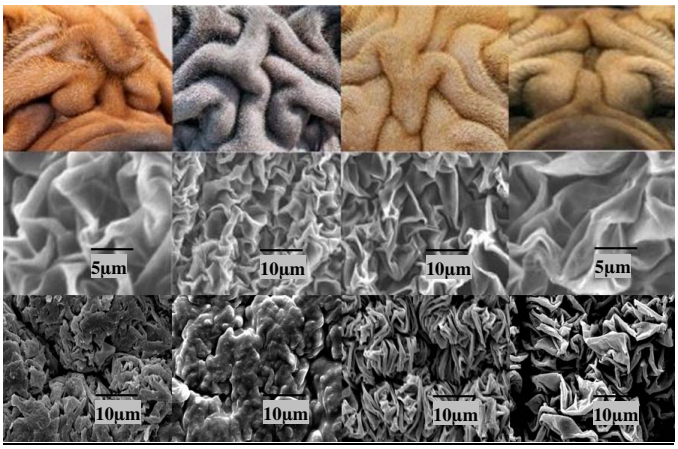

Fig. 1 The first row contains examples of the Shar-Pei dog images, while the second and third rows contain example images of the rGO SEM and MXene SEM images respectively.

B. Method

To quantify the similarity in the crumples observed in the 2D Shar-Pei dog images and the 2D SEM images, the following steps were performed:

1. Angle Extraction

The dog and sensor images were converted into grey scale images. Canny's edge detection method was used to extract the curves. Canny's edge detection method involves noise reduction using a Gaussian filter, finding the intensity gradient of the image, non-maximum suppression and hysteresis thresholding [19]. This algorithm contains several adjustable parameters which can affect the computation time and effectiveness of the algorithm. The adjustable parameters are the size of the Gaussian filter and the threshold used with hysteresis. Smaller Gaussian filter size causes less blurring and allows detection of small, sharp lines. A larger Gaussian filter causes more blurring, smearing out the value of a given pixel over a larger area of the image. A threshold set too high with hysteresis can miss important information. On the other hand, a threshold set too low will falsely identify irrelevant information (such as noise) as important. After several experiments, a threshold of 0.3 and a Gaussian filter size of 7 was found to be most useful for edge detection in this study.

This step resulted in a binary image with several curves identified because of edge detection. Connected component labeling was then adopted to identify each curve as a separate entity. Each curve was analyzed separately.

The first and last pixels of each curve were isolated. By browsing them between those two pixels, points of interest were set up along those curves. Finally, the angle between the points of interest was calculated using the atan2 function in MATLAB.

Figure 2 illustrates the angle extraction method adopted in this study. To summarize, the grayscale dog and SEM images were first loaded. The Canny edge detection method was used to obtain all the wrinkles in the images. To separate each curve, connected component labeling was applied. Then, each

curve was scanned to observe for change in orientation. The points where the change in orientation was observed were noted. The angle between the points where there was a change in orientation was calculated.

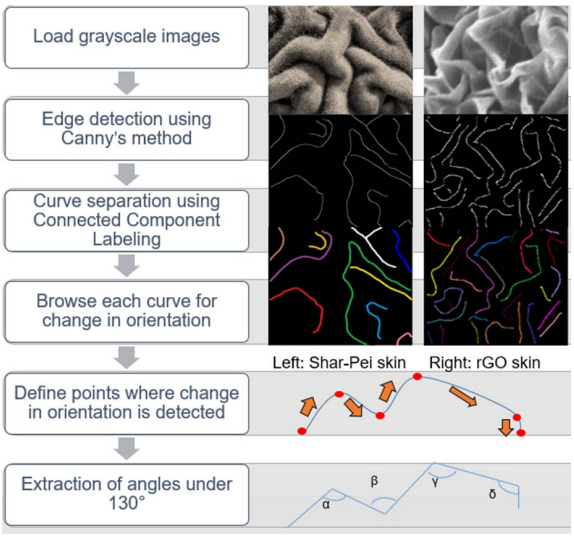

Fig. 2 Illustration of the pipeline of the study.

Figure 3 displays an example of the dog image used and manually labeled curves and angles considered in this study. The curves were manually segmented for illustration purpose in this figure and highlighted in red. The angles which were computed in this study are marked from 1-18 in white on the figure in the right.

Fig. 3 (Left) Illustration of an example dog image used in the study, (Right) Manually labelled curves in red along with the angles computed in this study.

Figure 4a shows the steps involved in the calculation of angles in every curve in dog and SEM image. Figure 4b and 4c show examples of angle calculation on arbitrary example images.

2. Similarity Analysis

A list of angles was obtained from each curve in the dog and SEM images. To compare the similarity in the 2D crumples between the dog skin and SEM images, the minimum, maximum, standard deviation, mean and median of the angles were calculated.

A histogram was plotted using the list of angles obtained from the SEM and dog images. An overlapping distribution of the angles computed from the SEM and dog images would imply that they have a similar distribution. Further, a boxplot was obtained to display the distribution of angles computed from the SEM and dog images. A similar median and inter-quartile range would indicate that the angles computed from the SEM and dog images are of similar distribution.

In order to visualize the possible resemblances between the distribution of the angles computed from the dog and SEM images, principal component analysis (PCA) was performed. If the scatter plot containing the principal component points from dog and SEM images are clustered together, it implies that the distribution of the angles computed from both sets of images is different.

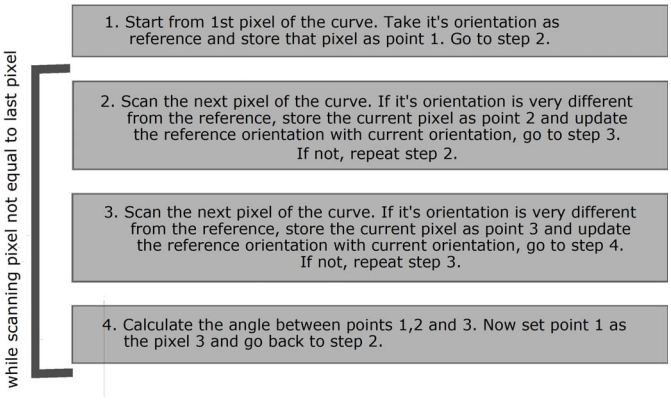

(a)

(b) (c)

Fig. 4 (a) Steps involved in the calculation of angles in every curve in dog and SEM image. (b-c) Illustration of angle calculation on arbitrary example images.

III. RESULTS AND DISCUSSION

After the list of angles from every curve from each dog and SEM image was calculated, a histogram was plotted to visualize the distribution of the angles obtained. Figure 5 shows the distribution of the angles calculated from each curve from every dog, rGO and MXene SEM images using a histogram. The x-axis represents the angles calculated in degrees, while the y-axis represents the count/frequency of each of the angle calculated from the dog, rGO and MXene SEM images. This plot shows that the distribution of the angles obtained from the SEM and dog images are overlapping to a high extent. This implies that the distribution of the angles computed from dog, rGO and MXene images have a similar statistical distribution.

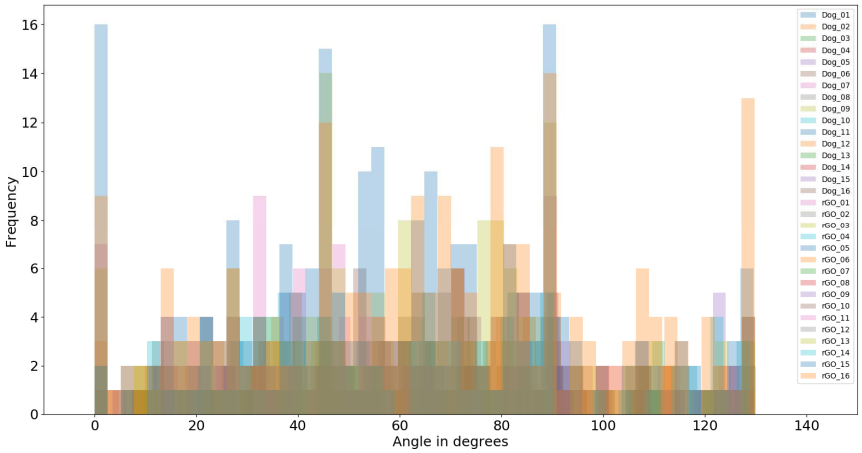

(a)

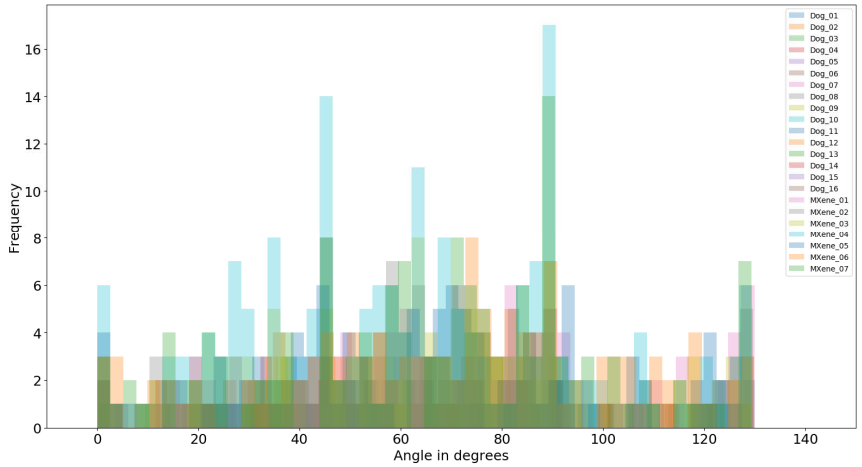

(b)

Fig. 5 (a) Illustration of the distribution of the angles calculated from each curve from every dog and rGO SEM image using a histogram. (b) Illustration of the distribution of the angles calculated from each curve from every dog and MXene SEM image using a histogram.

Along with the histogram, a boxplot was analyzed to illustrate the distribution of the angles calculated form every curve from each dog, rGO and MXene SEM image. Figure 6 shows the boxplot obtained. The median angle for every dog and SEM image is marked by the yellow line. The inter-quartile range is the 25th percentile to 75th percentile of the distribution of the angles for each of the dog and SEM image which is marked by the lower and upper boundary of the box

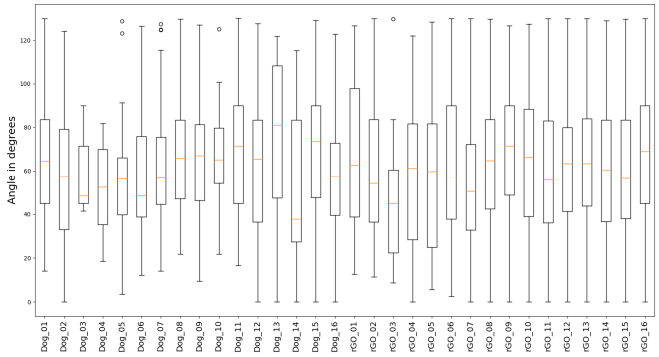

(a)

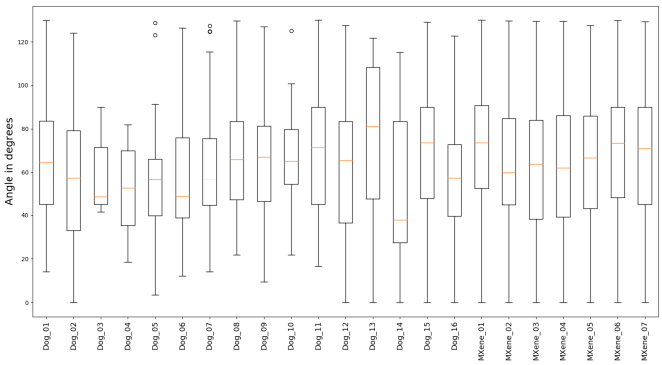

(b)

Fig. 6 (a) Illustration of the distribution of the angles calculated from each curve from every dog and rGO SEM image using a boxplot. (b) Illustration of the distribution of the angles calculated from each curve from every dog and MXene SEM image using a boxplot.

respectively. This figure shows that the median and the inter-quartile range of the angles in both dog and SEM images are similar, which implies that the angle distribution in both sets of images is similar.

Further, the mean, median, max, min and standard deviation (std) values of the angles were calculated for every dog, rGO and MXene SEM image. To visualize the possible resemblance in the wrinkled structure in SEM and dog images, principal component analysis (PCA) was performed using the five features computed - mean, median, max, min and std for every dog and SEM image. Figure 7 (a) shows the scatter plot of the first and second principal components from the dog and rGO images. The points for the 16 dog images are represented by blue cross marks, while the 16 rGO SEM images are represented by red circles. Figure 7 (b) shows the scatter plot of the first and second principal components from the dog and MXene SEM images. The points for the 16 dog images are represented by blue cross marks, while the 7 MXene SEM images are represented by red circles. It can be seen that the dog and SEM points on the plot are over-lapping and clustered together, which implies that the angle distribution in both sets of images is similar.

Figure 8 shows the scatter plot of the first and second principal components obtained after PCA using 3 features – mean, min and std from the dog, rGO and MXene SEM images. In figure 8 (a), the points for the 16 dog images are

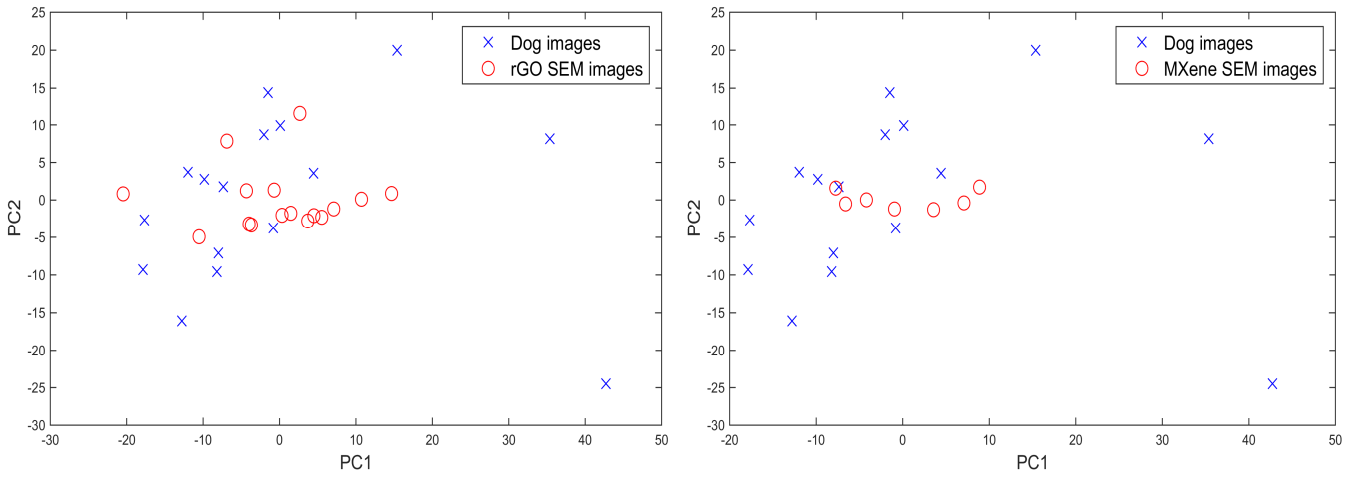

Fig. 7 (a) Scatter plot of the first 2 principal components obtained from principal component analysis using mean, median, min, max and std of the angles computed from the dog and rGO SEM images. (b) Scatter plot of the first 2 principal components obtained from principal component analysis using mean, median, min, max and std of the angles computed from the dog and MXene SEM images.

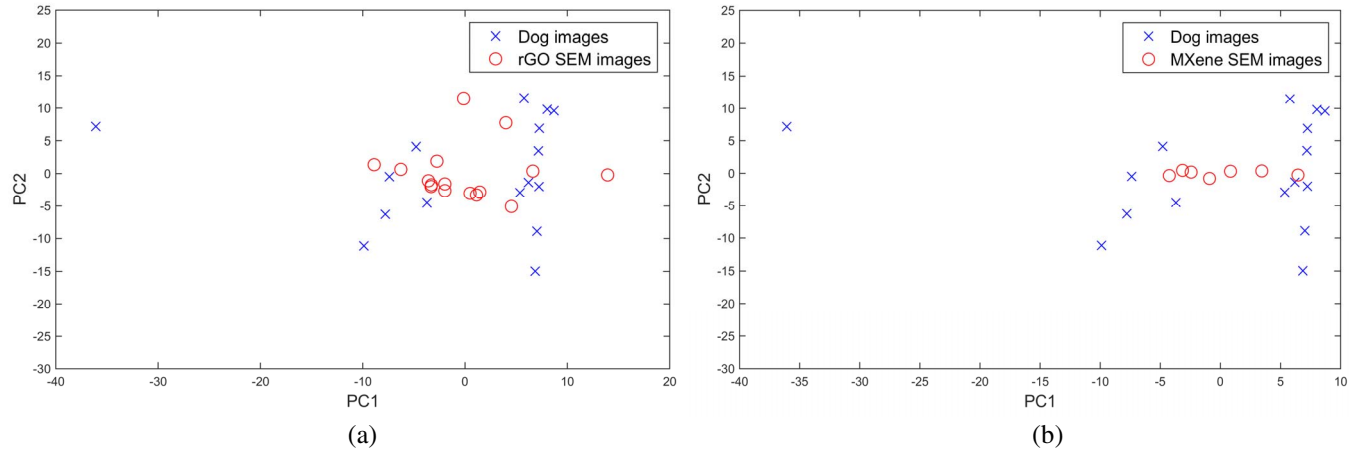

Fig. 8 (a) Scatter plot of the first 2 principal components obtained from principal component analysis using mean, median and std of the angles computed from the dog and rGO SEM images. (b) Scatter plot of the first 2 principal components obtained from principal component analysis using mean, median, min, max and std of the angles computed from the dog and MXene SEM images.

represented by blue cross marks, while the 16 rGO SEM images are represented by red circles. In figure 8 (b), the points for the 16 dog images are represented by blue cross marks, while the 7 MXene SEM images are represented by red circles. It can be seen that the dog and SEM points on the plot are over-lapping and clustered together, which implies that the angle distribution in both sets of images is similar.

Hence, this work demonstrates evidence of the topographical similarity between dog face patterns and the patterns in the SEM images.

In our future work, we aim to investigate multiple other biomimetic parameters, such as surface smoothness, stretchability or stiffness, and number of curvatures which could possibly provide more insight into explaining how the nature-inspired sensor may obtain a superior performance.

IV. Conclusion

This study aims to examine the biomimetic similarity of the wrinkle patterns of the stretchable electrodes that we intend to use in robots, with images of Shar Pei dog. The similarities in the wrinkle structures were analyzed by computing the angles of the ripples and curves in the SEM images. The distribution of the angles computed from SEM and dog images were found to have similar distribution. Using this methodology, we have established the biomimetic geometrical similarity of SEM images of the wrinkled patterns of the stretchable 2D material electrodes with the Shar-Pei stretchable skin patterns. Using the similarity in mechanical structure, we hope to be able to explain how the biomimetic patterns can contribute to the stretchability and sensing properties of the pressure sensor.

ACKNOWLEDGEMENT

This work is supported by the Singapore NMRC Bedside Bench under grant R-397-000-245-511 awarded to Dr. Hongliang Ren.

References

[1] R. L'Orsa, C. Macnab and M. Tavakoli, "Introduction to Haptics for Neurosurgeons", Neurosurgery, vol. 72, pp. A139-A153, 2013.

[2] P. Puangmali, K. Althoefer, L. Seneviratne, D. Murphy and P. Dasgupta, "State-of-the-Art in Force and Tactile Sensing for Minimally Invasive Surgery", IEEE Sensors Journal, vol. 8, no. 4, pp. 371-381, 2008. Available: 10.1109/jsen.2008.917481.

[3] C. Wagner, N. Stylopoulos and R. Howe. "The role of force feedback in surgery: analysis of blunt dissection" in 10th Symposium on Haptic Interfaces for Virtual Environment and Teleoperator Systems Proceedings, 2002, pp. 68-74.

[4] G. Tholey, J. Desai, and A. Castellanos. "Force feedback plays a significant role in minimally invasive surgery: results and analysis" Annals of surgery, 2005, pp. 102.

[5] M. Tavakoli, A. Aziminejad, R. Patel and M. Moallem, "High-Fidelity Bilateral Teleoperation Systems and the Effect of Multimodal Haptics", IEEE Transactions on Systems, Man, and Cybernetics, Part B (Cybernetics), vol. 37, no. 6, pp. 1512-1528, 2007. Available: 10.1109/tsmcb.2007.903700.

[6] M. Tiwana, S. Redmond and N. Lovell, "A review of tactile sensing technologies with applications in biomedical engineering", Sensors and Actuators A: Physical, vol. 179, pp. 17-31, 2012. Available: 10.1016/j.sna.2012.02.051.

[7] B. Ahn et al., "Omnidirectional Printing of Flexible, Stretchable, and Spanning Silver Microelectrodes", Science, vol. 323, no. 5921, pp. 1590-1593, 2009. Available: 10.1126/science.1168375.

[8] J. Yang, Y. Ye, X. Li, X. Lü and R. Chen, "Flexible, conductive, and highly pressure-sensitive graphene-polyimide foam for pressure sensor application", Composites Science and Technology, vol. 164, pp. 187-194, 2018. Available: 10.1016/j.compscitech.2018.05.044.

[9] P. Chen, M. Liu, Z. Wang, R. Hurt and I. Wong, "From Flatland to Spaceland: Higher Dimensional Patterning with Two-Dimensional Materials", Advanced Materials, vol. 29, no. 23, p. 1605096, 2017. Available: 10.1002/adma.201605096.

[10] S. Kim, K. Choi, B. Lee, Y. Kim and B. Hong, "Materials for Flexible, Stretchable Electronics: Graphene and 2D Materials", Annual Review of Materials Research, vol. 45, no. 1, pp. 63-84, 2015. Available: 10.1146/annurev-matsci-070214-020901.

[11] M. Hammock, A. Chortos, B. Tee, J. Tok and Z. Bao, "25th Anniversary Article: The Evolution of Electronic Skin (E-Skin): A Brief History, Design Considerations, and Recent Progress", Advanced Materials, vol. 25, no. 42, pp. 5997-6038, 2013. Available: 10.1002/adma.201302240.

[12] N. Luo et al., "Flexible Piezoresistive Sensor Patch Enabling Ultralow Power Cuffless Blood Pressure Measurement", Advanced Functional Materials, vol. 26, no. 8, pp. 1178-1187, 2015. Available: 10.1002/adfm.201504560.

[13] R. Nur, N. Matsuhisa, Z. Jiang, M. Nayeem, T. Yokota and T. Someya, "A Highly Sensitive Capacitive-type Strain Sensor Using Wrinkled Ultrathin Gold Films", Nano Letters, vol. 18, no. 9, pp. 5610-5617, 2018. Available: 10.1021/acs.nanolett.8b02088.

[14] S. Park, J. Kim, M. Chu and M. Khine, "Flexible Piezoresistive Pressure Sensor Using Wrinkled Carbon Nanotube Thin Films for Human Physiological Signals", Advanced Materials Technologies, vol. 3, no. 1, p. 1700158, 2017. Available: 10.1002/admt.201700158.

[15] X. Hu, Y. Dou, J. Li and Z. Liu, "Buckled Structures: Fabrication and Applications in Wearable Electronics", Small, vol. 15, no. 32, p. 1804805, 2019. Available: 10.1002/smll.201804805.

[16] T. Chang, Y. Tian, C. Li, X. Gu, K. Li, H. Yang, P. Sanghani, C. M. Lim, H. Ren, and P.-Y. Chen, "Stretchable Graphene Pressure Sensors with Shar-Pei-like Hierarchical Wrinkles for Collision-Aware Surgical Robotics", ACS Applied Materials & Interfaces, vol. 11, no. 10, pp. 10226–10236, 2019.

[17] J. Finch, S. Abrams, and A. Finch, "Analogs of human genetic skin disease in domesticated animals", International Journal of Womens Dermatology, vol. 3, no. 3, pp. 170–175, 2017.

[18] P.-Y. Chen, J. Sodhi, Y. Qiu, T. M. Valentin, R. S. Steinberg, Z. Wang, R. H. Hurt, and I. Y. Wong, "Graphene Topographies: Multiscale Graphene Topographies Programmed by Sequential Mechanical Deformation (Adv. Mater. 18/2016)", Advanced Materials, vol. 28, no. 18, pp. 3603–3603, 2016.

[19] J. Canny, "A Computational Approach to Edge Detection", Readings in Computer Vision, pp. 184–203, 1987.